J. Cent. South Univ. (2021) 28: 1219−1232
DOI: https://doi.org/10.1007/s11771-021-4691-0

Springer

Microstructure and properties of Al-doped ODS steels prepared by wet-milling and SPS methods

SUN Yu-zhou(孙煜舟)[1], LIN Nan(吝楠)[1, 2], ZHANG Wu-jun(章伍军)[1], ZHANG Yong-sen(张永森)[1], LI Zhong-tao(李忠涛)[1], HAN Xian-qi(韩现奇)[1], WU Zheng-gang(吴正刚)[1], WANG Zu-yong(王祖勇)[1], MA Chao(马超)[1]

1. College of Materials Science and Engineering, Hunan University, Changsha 410082, China;
2. National Key Laboratory of Science and Technology on High-strength Structural Materials, Central South University, Changsha 410083, China

Abstract: In this paper, 15Cr-ODS steels containing 0, 1 wt%, 2 wt% and 3 wt% Al element were fabricated by combining wet-milling and spark plasma sintering (SPS) methods. The microstructure and mechanical properties of ODS steel were investigated by XRD, SEM, TEM, EBSD and tensile tests. The results demonstrate that the Al addition significantly refines the particle precipitates in the Fe-Cr matrix, leading to the obvious refinement in grain size of matrix and the improvement of mechanical properties. The dispersion particles in ODS steels with Al addition are identified as Al_2O_3 and $Y_2Ti_2O_7$ nanoparticles, which has a heterogeneous size distribution in the range of 5 nm to 300 nm. Increasing Al addition causes an obvious increase in tensile strength and a decline in elongation. The tensile strength and elongation of 15Cr-ODS steel containing 3 wt% Al are 775.3 MPa and 15.1%, respectively. The existence of Al element improves the corrosion resistance of materials. The ODS steel containing 2 wt% Al shows corrosion potential of 0.39 V and passivation current density of 2.61×10^{-3} A/cm^2(1.37 V). This work shows that Al-doped ODS steels prepared by wet-milling and SPS methods have a potential application in structural parts for nuclear system.

Key words: wet-milling; spark plasma sintering; ODS steels; oxide nanoparticles; microstructure; tensile strength; dispersion strengthening

Cite this article as: SUN Yu-zhou, LIN Nan, ZHANG Wu-jun, ZHANG Yong-sen, LI Zhong-tao, HAN Xian-qi, WU Zheng-gang, WANG Zu-yong, MA Chao. Microstructure and properties of Al-doped ODS steels prepared by wet-milling and SPS methods [J]. Journal of Central South University, 2021, 28(4): 1219−1232. DOI: https://doi.org/10.1007/s11771-021-4691-0.

1 Introduction

In recent years, the development of IV-generation fission reactors and commercial nuclear fusion reactors has become increasingly urgent due to the requirement of clean energy. However, the cladding material used in nuclear fission reactors and the first wall material in fusion reactors still need the superior performance [1, 2]. Owing to the excellent irradiation resistance and high-temperature mechanical properties [3−6], oxide dispersion strengthened (ODS) steels, which have been developed rapidly since 1970s, are considered the most promising cladding material in supercritical pressurized water reactor (SCPWR), sodium-cooled fast reactor (SFR), and lead bismuth-cooled fast reactor (LFR). The traditional ODS steels have a concentration of chromium ranged between 9 wt% and 20 wt%. However, it was pointed out by many previous studies that ODS steels containing 14 wt%−16 wt% Cr have excellent corrosion resistance and

Foundation item: Project(2020JJ2001) supported by Outstanding Youth Scientist Foundation of Hunan Province, China; Project(6142912200102) supported by Foundation for National Key Laboratory of Science and Technology on High-strength Structural Materials, China
Received date: 2021-01-10; **Accepted date:** 2021-04-15
Corresponding author: MA Chao, PhD, Professor; Tel: +86-731-88821611; E-mail: cma@hnu.edu.cn; ORCID: https://orcid.org/0000-0001-8599-9340

aging embrittlement [3]. It is also noted that the aluminum addition during the fabrication process is a key factor to increase the corrosion resistance of ODS steels [3, 7, 8]. In this case, the Y-Ti-O nano-precipitates are easily replaced by Y-Al-O particles due to the high chemical activity of Al. The Y-Al-O particles with $Y_4Al_2O_9$, $YAlO_3$ and $Y_3Al_5O_{12}$ crystal structure are coarser than that with Y-Ti-O particles, leading to a decrease in the mechanical property of matrix [9−13]. The Y-Al-O nanoparticles with core-shell structure can be generated in MA956 (20Cr-4.5Al) and 16Cr-4.5Al ODS steels through a three-stage forming mechanism, including fragmentation of starting Y_2O_3 particles, agglomeration and solid-state amorphization of Y_2O_3 fragments, and the crystallization of nanoparticles [12]. The studies about the effect of Cr content on the corrosion behavior in Al-added ODS steels revealed that high Cr concentration would result in significant improvement in the corrosion resistance [3]. The size and number density of oxide particles in Al-added ODS steel mainly depend on the fabrication process. It was proposed by previous studies that Y-Al-O particles incline to precipitate in the form of complex compounds at the subsequent hot extrusion process [14]. The heat treatment at high temperature over 1150 °C can cause the coarsening of oxide particles [15]. Due to the Al addition induced enhancement of corrosion resistance, the Al-doped ODS steels possess a promising outlook for application of structural materials in the extreme environment. However, the influence of varied Al addition on nano-sized particles, grain size distribution and mechanical properties should be explored systemically.

As we all know, the key characteristic of ODS steels is the existence of uniformly distributed nano/ultrafine Ti-O, Y-Ti-O, and Y-Al-O oxide particles, which remains the excellent thermal stability under high temperature (over 1300 °C) [16]. The rich interfaces between the matrix and oxide particles provide a large number of defects to capture vacancies, helium bubbles and emergent defects in neutron irradiation environment, and preventing the primary defects from gathering and coarsening at grain boundary. Additionally, the dispersed oxide particles could also act as pinning points to restrain the movement of dislocations during the deformation and thus improve the mechanical properties of matrix. All of these features clearly demonstrate that the mechanical properties of ODS steels depend on the chemical composition, microstructure, and distribution of oxide particles. The aberration-corrected scanning transmission electron microscope (STEM) with atomic resolution can be used to well characterize the microstructure of oxide particles and reveal the relationship between structure and properties in ODS steels.

To fabricate the ODS steel raw powders, the traditional method is the mechanical alloying of various powders through the high-energy ball milling [17−19]. A typical high-energy ball milling method is usually carried out in argon or nitrogen atmosphere for preventing oxidation phenomenon during the ball milling process. This method would cause a violent squeeze and deformation of alloy powders between the steel ball and mill pot, thus a cold welding of powders. Another drawback is the impurity contamination of milling powder from the ball and bowl. The elevated temperature during the milling can induce an increase in the oxygen content of mixed powders. Therefore, commercial ODS steels powders prepared by the high-energy ball milling method still have some problems which need to be resolved. The wet milling process is a typical powder metallurgy method that has been used in preparing as-milled powder and alloy. During the wet-milling process, the added alcohol medium can reduce the temperature of powder and inhibit the introduction of impurity contamination. In addition, the requirements of manufacturing facility in wet-milling process are simpler than that in high-energy ball milling process. At present, the wet-milling method has been used in the industrial preparation of hardmetals, cermet and high speed steel [20−22]. Therefore, this method may be conducive to the large scale production of high-performance ODS steels. However, it has not been applied to the preparation of ODS steels so far. The aim of this paper is to investigate the preparation of ODS steels by the wet-milling method and the effects of Al additions on the microstructure, mechanical properties and corrosion resistance of sintered ODS steels.

2 Experimental procedure

A series of 15Cr-ODS steels with 0, 1 wt%, 2 wt% and 3 wt% Al addition were manufactured by a wet-milling process and spark plasma sintering

(SPS) method. The nominal compositions of ODS steels with different Al content are listed in Table 1. The various raw powders were mixed in ethyl alcohol media with a high-energy planetary mill (XQM-2, Changsha TENCAN powder Co. Ltd.) for 48 h. The rotation speed and ball-to-powder mass ratio were 250 r/min and 5:1, respectively. Subsequently, the mixed powders were firstly heated to 800 °C for 5 min, and then continuously heated to 1100 °C for a 10 min sintering in LABOX-325R sintering system with a pressure of 40 MPa under vacuum environment. Finally, the sintered alloys were ground and polished by the aluminium oxide paste and polishing agent.

Table 1 Nominal compositions of ODS steels with different Al content (wt%)

ODS-steel	Fe	Cr	Al	W	Ti	Y_2O_3
15Cr	Bal.	15	—	2	0.4	0.25
15Cr1Al	Bal.	15	1	2	0.4	0.25
15Cr2Al	Bal.	15	2	2	0.4	0.25
15Cr3Al	Bal.	15	3	2	0.4	0.25

The density of sintered 15Cr-ODS steel was tested by Archimedes principle, and the theoretical density was calculated by the following equation [23]:

$$\frac{1}{\rho}=\frac{\omega_1}{\rho_1}+\frac{\omega_2}{\rho_2}+\frac{\omega_3}{\rho_3}+\cdots+\frac{\omega_i}{\rho_i} \quad (1)$$

where ρ, ρ_i and ω_i are the theoretical density of the alloy, the densities of pure alloy and the corresponding mass fractions, respectively. The crystal structure and phase component of the mixed powder and sintered alloy were examined by X-ray diffraction (XRD) measurements with a scan rate of 10 (°)/min. SEM images of microstructure and fracture surface of ODS steels were taken from a TESCAN MIRA3-LMH scanning electron microscope (SEM) equipped with Oxford X MAX20 energy dispersive spectrometer (EDS). The TEM and STEM measurements were carried out by using a JEOL ARM-200F microscope which is operated at 200 kV and equipped with a probe-forming aberration corrector. Tensile tests of materials were performed in a screw-driven tensile testing machine (SHIMADZU AGS-X 50KN) at an engineering strain rate of 1×10^{-3} s^{-1} at room temperature. The grain size and distribution of ODS steels were observed and measured by Hitachi S-3400N SEM equipped with EDAX-TSL electron backscatter diffraction (EBSD) instrument. Electrochemical experiments of Al-doped 15Cr ODS steels were executed with a potentiostat unit (CHI660E) in 1 mol/L HNO_3 solution at 55 °C. The potentiodynamic polarizations tests were performed at a constant scan rate of 0.01 V/s and the scans potentials were started from −1.2 V to 2.0 V.

3 Results and discussion

3.1 Phase and chemical composition

To investigate the phase composition variation of ODS steel powders during the process of ball-milling and sintering, the phases of mixed powder and sintered alloy were measured by XRD measurements. The XRD data of mixed powders with 3 wt% Al addition and sintered ODS steels are shown in Figure 1(a). The peaks corresponding to Fe, W and Al crystals can be clearly seen in the

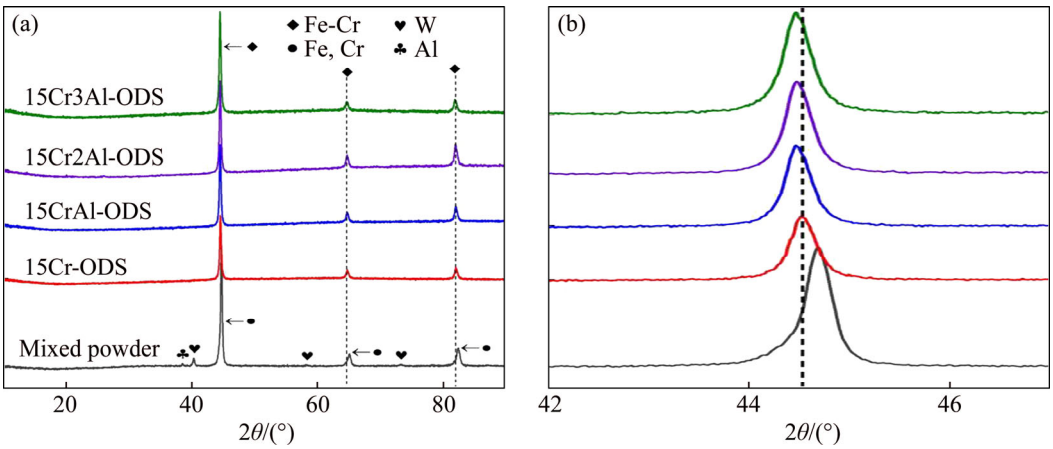

Figure 1 XRD patterns of mixed steel powder with 3% Al addition and sintered ODS steels with different Al contents (a) and enlarged XRD pattern (b)

pattern of mixed powder before sintering, which clearly demonstrates that no new phases were formed during the ball milling process. It should be noted that the peaks corresponding to Cr crystal are close to those of Fe crystal due to their similar lattice constants. Moreover, Cr content in the alloy is much less than Fe content, so Cr peaks cannot be observed in the XRD pattern obviously. In the sintered ODS steel, the XRD result shows a pure Fe-Cr phase with BCC structure, indicating that Cr and W elements have dissolved into the Fe matrix and a new Fe-Cr phase was formed during the sintering process. The lattice parameters of matrix become large due to the dissolved atoms in Fe lattice, and thus the peaks corresponding to Fe-Cr phase shift to low angle compared with the Fe peaks in mixed powder, as shown in enlarged XRD pattern in Figure 1(b). Additionally, with the addition of extra Al element, the peaks of Fe-Cr phase in ODS alloy shift to the low angle slightly, which means that the aluminum element with the large atomic radius dissolves into matrix during sintering process.

In the traditional mechanical alloying method, various raw material powders are directly squeezed and crushed by steel balls in the dry milling process. New phase would be formed in the mixed powders during the milling stage of the mechanical alloying, which has been confirmed by many previous studies [24−26]. In this work, the mixed powders were prepared by the wet milling process in alcohol medium. The powder extrusion, crushing and cold welding in the wet milling process are not as intensive as those in the dry milling, so it is favorable to prevent the formation of new phase.

The morphology and EDS analysis results of different Al-doped ODS steels were characterized by SEM, as shown in Figure 2. The second phase precipitates in 15Cr ODS steel without Al addition show the heterogeneous distribution and coarse particle size. The EDS spectra taken from different points reveal that particles 1 and 2 marked in 15Cr ODS alloy are mainly rich in Ti, Cr, and O elements, indicating that these coarse precipitates may be Ti-Cr-O particles. It has been reported in the previous studies that large $CrTiO_3$ precipitates phase usually appeared in the matrix of ODS alloy [27, 28]. In addition, LU et al [29] have systematically studied the oxide dispersions in ODS alloy and identified Ti-Cr-O precipitates as $TiCr_2O_4$ phase with a spinal structure. As shown in Figures 2(b)−(d), with the elevated Al addition, the particles in 15Cr3Al ODS alloy tend to be refined obviously, indicating that Al addition could significantly refine the grain size of precipitates. Furthermore, the density of dispersed particles is also increased with the elevated Al content. EDS results from particles 3 and 4 as marked in 15Cr3Al ODS steel show that the dispersed particles with high Al content belong to aluminum oxides. Additionally, the EDS results of matrix in different Al-doped alloys show that the extra Al element dissolves into the matrix. With the elevated Al content, the aluminum contents in the matrix increase continuously.

3.2 Chemical composition and atomic structure of oxide nanoparticles

The high-angle annular dark-field (HAADF) STEM image for the specimen with 1% Al addition clearly displays the morphology and distribution of oxide particles which appear as dark contrast, as shown in Figures 3(a) and (b). These oxide particles, with the particle size in the range between 5 and 300 nm, are mainly located inside the grain rather than at the grain boundary. Small oxide particles less than 100 nm are basically in spherical shape, while the large precipitates are usually irregular. Combing high-magnification STEM images and elemental mappings, it is found that these irregular-shaped precipitates shown in HAADF image are actually formed by the accumulation of multiple spherical particles. It should be noted that the large second-phase precipitate would introduce a stress concentration at the interface and become vulnerable to the strain. This feature is not favorable for improving the mechanical property of ODS steels, and thereby precipitate coarsening should be avoided during the powder milling and sintering process.

Figure 3(c) displays the X-ray EDS elemental mappings for Fe, Cr, Al, Y, Ti, and O elements. It can be clearly seen that the majority of oxide particles are composed of Al and O elements and the rest are composed of Y, Ti, and O elements, indicating the coexistence of aluminum oxides (red arrows) and yttrium titanium oxides particles (green arrows) in the used sample. In addition, the titanium oxides particles composed of only Ti, and O elements are also observed, as indicated by the blue arrow in Figure 3(a). The overlapping of different elements suggests that the large irregular-shaped precipitates consist of more than one type of oxide particles.

Due to multiple phases in Y-Ti-O and Al-O oxides, the elemental mappings can only provide

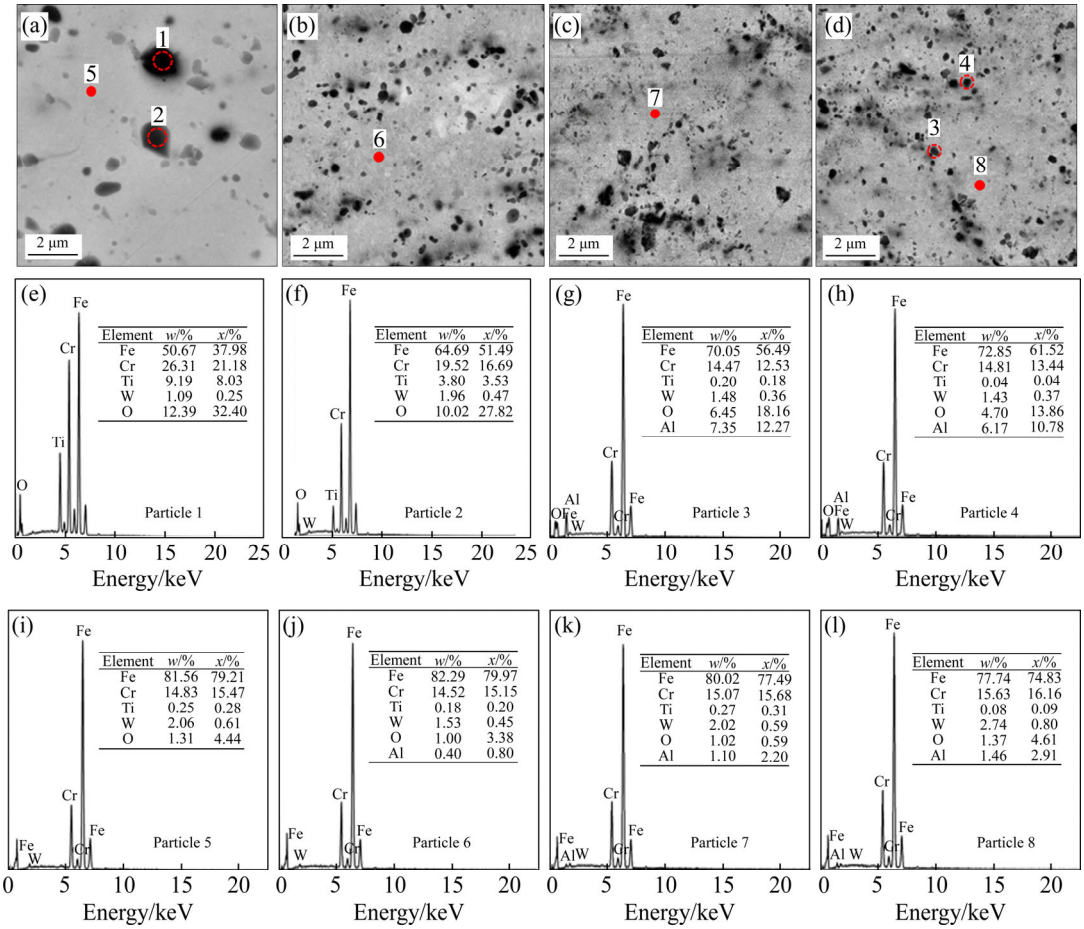

Figure 2 BSE-SEM micrograph of 15Cr (a), 15Cr1Al (b), 15Cr2Al (c) and 15Cr3Al (d) ODS steels and corresponding EDS results (e−l) detected in particles 1-4 and point 5-8, respectively

chemical composition of oxide particles. Here, in order to further identify the specific phase and atomic structure of different oxide particles, atomic-resolution HAADF-STEM images were taken from different particles, as shown in Figure 4. Figures 4(a)−(c) display a HAADF image taken from the Y-Ti-O particle labeled by particle 1 and the corresponding fast Fourier transformation (FFT). By indexing the primary spots in the FFT, this particle can be determined to be $Y_2Ti_2O_7$ with pyrochlore structure. The structure model of $Y_2Ti_2O_7$ is superimposed in the HAADF image in which both columns' positions and intensities agree well with the structure model. The simulated electron diffraction pattern from the structure model is also well consistent with the FFT of HAADF image. By using the same method, the Al-O particles are identified to be Al_2O_3 of rhombohedral structure, as shown in Figures 4(d)−(f).

In previous studies [14, 30, 31], many researchers have also discovered $Y_2Ti_2O_7$ and Al_2O_3 particles in ODS steels. However, it is worth noting that in Al added ODS alloys, the chemically active aluminum will replace titanium to form Y-Al-O oxide with larger sizes rather than Y-Ti-O particles, and thus reduce mechanical properties, as proposed by previous studies. However, in this work, despite the addition of Al element, the TEM characterizations clearly demonstrated that the Y-Ti-O oxide particles still appear and no Y-Al-O particles were found. Considering the introduction of wet milling process used here to prepare ODS alloy, which is different from dry milling in the protected Ar atmosphere, it may be a new road to fabricate Al added ODS steels with excellent mechanical properties.

3.3 Effect of Al-additions on grain size and mechanical properties

EBSD technology is generally used to analyze the grain size and distribution of Fe-Cr grains in ODS steels. Figure 5 displays the EBSD grain orientation maps (inverse pole figure X, IPFX) of the

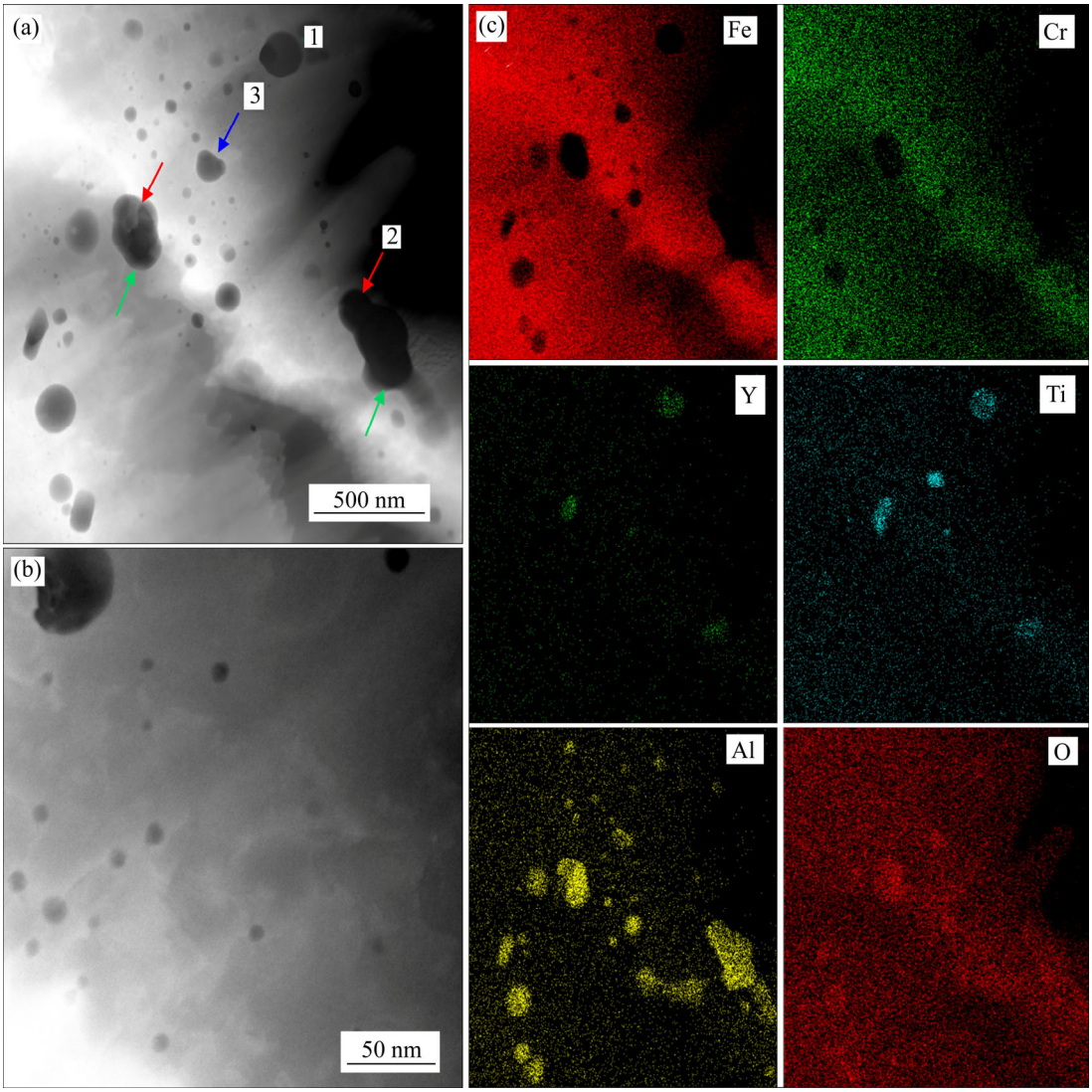

Figure 3 Low-magnification HAADF-STEM image (a), enlarged image (b) and (c) EDS elemental mappings for Fe, Cr, Al, Y, Ti, and O elements of 15Cr1Al-ODS alloy

obtained ODS steels with different Al additions, in which different grain orientations are represented by different colored areas. It can be seen that increasing Al contents lead to the decreased grain size and the uniform distribution of grains in Fe-Cr matrix. As shown in Figures 5(a) and (b), the EBSD map of the samples without and with 1 wt% Al additions exhibit plenty of fine grains around the coarse ones. The morphology with nonuniformity grain size and bimodal grain distribution is attributed to the rapid growth of grains during SPS sintering process and the lack of pinning from oxide particles in matrix without Al addition. Under high temperature and high pressure, the growing grains and their adjacent fine grains would merge to large grains rapidly. Figures 5(c) and 5(d) show the EBSD maps of the ODS steels with 2 wt% and 3 wt% Al additions, respectively. As Al powder is increased, the grains of ODS steel have an obvious refinement and a uniform distribution. The addition of Al powders causes the generation of numerous oxide particles in ODS steel matrix, which largely prevents the grain boundary from migrating during grain growth in sintering process.

Based on the EBSD analysis, the influence of Al addition on the average grain size of ODS steel matrix is studied, as shown in Figure 6. The average grain size of steel matrix is decreased significantly with the increase of Al content. However, it is worth noting that the average grain size of steel matrix tends to increase slightly when Al content exceeds 2 wt%. This phenomenon may be due to the aggregation and coarsening of Al-containing oxides, which reduces the ability of particles to hinder the

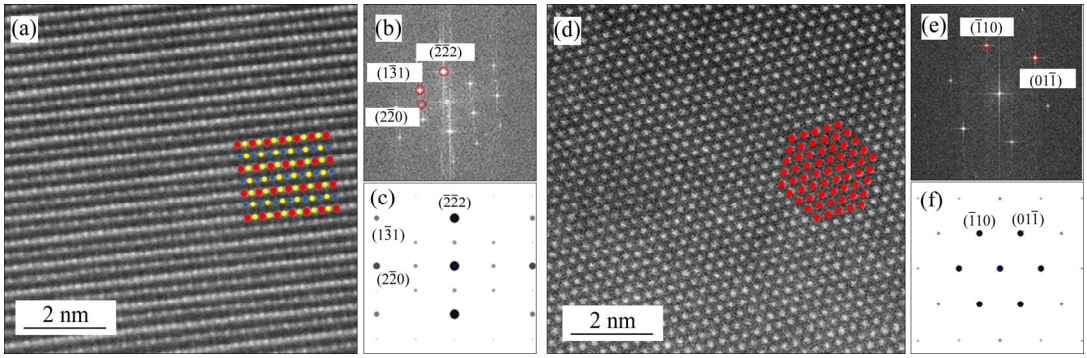

Figure 4 STEM-HAADF image with structure model of particles1 and 2 marked in Figure 3 (a, d) and corresponding FFT pattern (b, e) and simulated electron diffraction pattern (c, f) in 15Cr1Al-ODS alloy. (The red, blue and yellow dots in structure model of $Y_2Ti_2O_7$ represent the atom column of Y, Ti and alternating Y and Ti, respectively. The red dot represents the atom column of Al in the structure model of Al_2O_3)

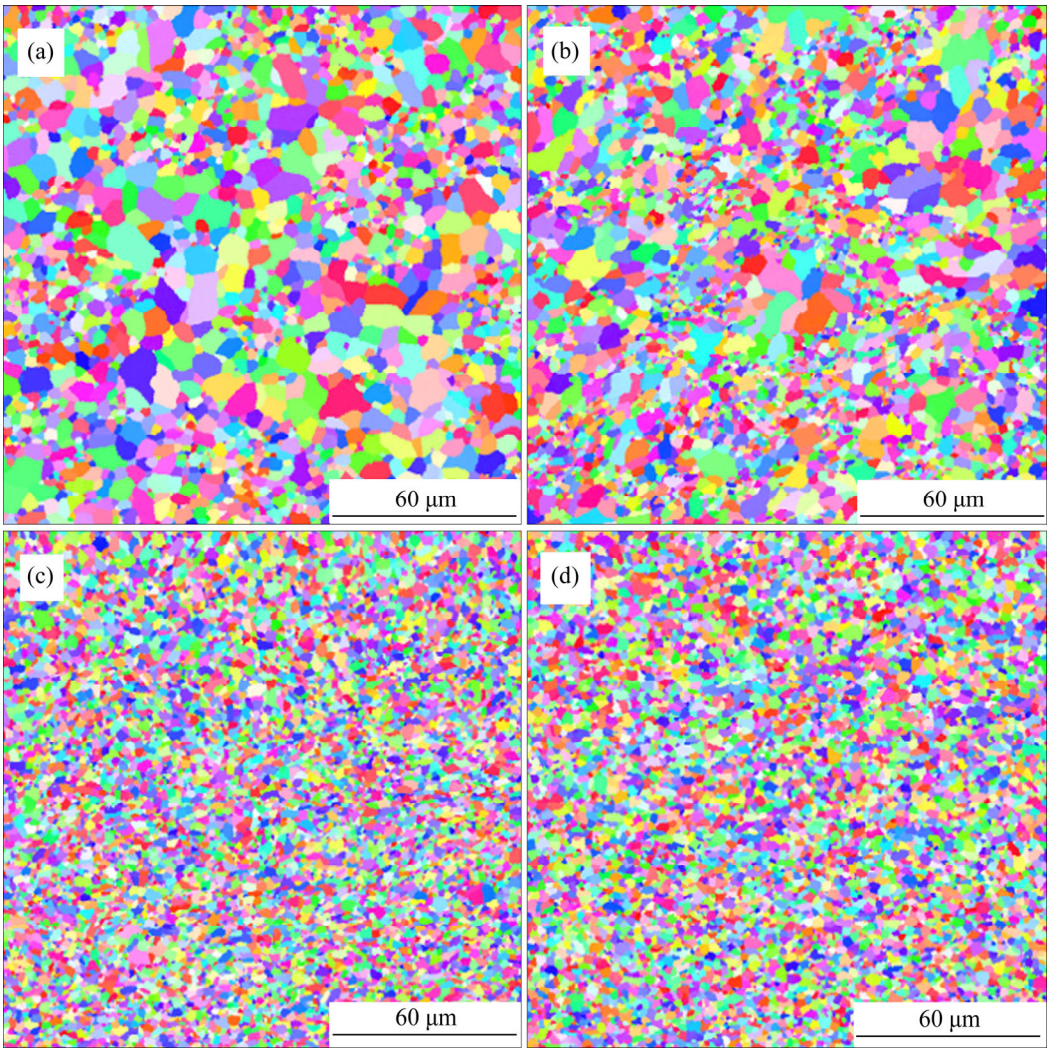

Figure 5 EBSD maps with different grain orientation in ODS steels with 0 (a), 1 wt% (b), 2 wt% (c), 3 wt% (d) Al additions

movement of grain boundary and growth of grains. In fact, the introduction of second-phase particles in alloy is an effective method for refining grains of materials and improving the mechanical properties. The grain size of matrix depends on the size and volume fraction of second-phase particles, and their relationship should follow the Zener-Smith formula [32]:

$$R=\frac{4r_p}{3f_v} \quad (2)$$

where R and r_p represent respectively the radius of matrix grains and second phase particles, and f_v represents the volume fraction of second-phase particles in the matrix. According to Eq. (2), when second-phase particle size remains a constant, the size of matrix grain is decreased as the oxide particle content is increased. As mentioned above, a considerable number of second-phase particles generated in Al added ferrite matrix hinder the movement of grain boundary. Therefore, the existence of these second-phase particles would restrict the migration of grain boundaries and dislocations, and thus lead to uniform fine grains in the ODS steels with Al addition.

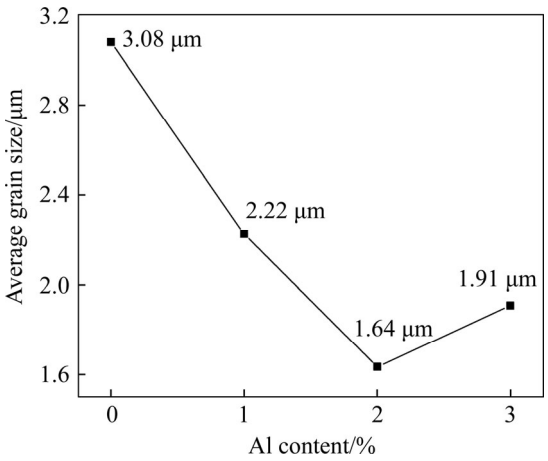

Figure 6 Average grain size of matrix in ODS steel with different Al contents

On the other hand, the Al addition would change the relative density and tensile strength which are important for the mechanical property of ODS steels. The relative density of 15Cr-ODS steel without Al additions fabricated by spark plasma sintering is 97.7%. With increasing Al content, the relative density of ODS steels is increased gradually. The relative density of 15Cr-ODS steel containing 1 wt% and 2 wt%Al is 98.1% and 99.2%, respectively. When Al content is increased up to 3 wt%, the relative density can reach to 99.8%. During the spark plasma sintering, the densification process of mixed powders depends on the solid phase diffusion of elements and the rearrangement of particles under high temperature and high pressure. The existence of refined and uniform matrix grains induced by ultrafine oxides particles is beneficial for the rearrangement of grains during sintering process. The rich interfaces in refined matrix grains enhance the element diffusion at high temperature and improve the density of ODS steels. Figure 7 shows the ultimate tensile strength (UTS) and total elongation (TE) of 15Cr-ODS steels with different Al contents. The tensile strength of ODS steels without Al addition is 582 MPa. With increasing Al content, the tensile strength of material containing 3 wt% Al is increased up to 775.3 MPa. However, by comparing with the Al-free ODS steel, the elongation of the ODS steel containing 3 wt% Al element is decreased from 28.1% down to 15.1%. As a commercial Al added ODS steel produced by Special Metals Corporation in the United States [33], MA956 (20Cr-4.5Al) has very similar chemical composition with 15Cr3Al ODS steel used in this work. The tensile strength and elongation of MA956 are 630 MPa and 10%, respectively. The 15Cr3Al ODS steel here prepared by wet-milling and SPS method has better mechanical property than MA956, suggesting that the wet milling method is a feasible and effective method to prepare the high-performance ODS steels.

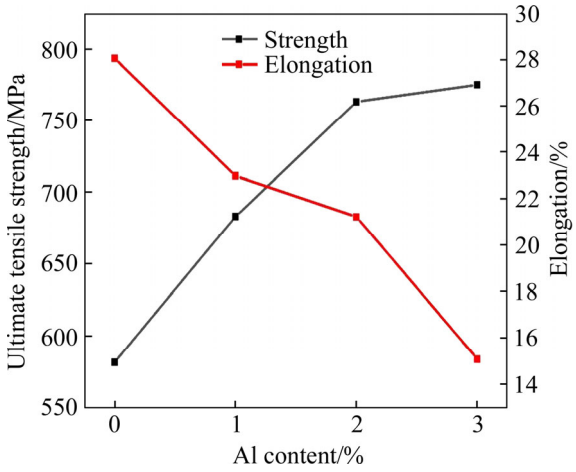

Figure 7 Ultimate tensile strength and total elongation of 15Cr-ODS steels with different Al contents

Besides a large number of Al_2O_3 particles with a size of 5−300 nm in the Fe-Cr matrix with Al addition, numerous small Y-Ti-O particles were observed due to the reaction between Ti and Y_2O_3 during the SPS sintering. SEM and TEM images clearly show the morphology and distribution of this kind of particles which play an important role on the mechanical property of ODS steels. According to the Orowan bypass mechanism, cutting or bypassing dispersed fine oxide particles by dislocations needs additional energy and can increase the strength of

ODS alloys [34]. The contribution of these oxide particles to the increment of strength can be expressed as [34]:

$$\Delta\sigma_{\text{Orowan}}=\frac{0.13G_{\text{m}}b}{\lambda}\ln\frac{d_{\text{p}}}{2b} \tag{3}$$

where G_{m} is the shear modulus for ferrite (80 GPa); b is the Burgers vector of matrix (0.248 nm); d_{p} is the average diameter of particles; and λ is the mean inter-particle distance of dispersed particles in matrix. As mentioned above, when the alloy is under plastic deformation, a large number of oxide particles in the ODS steel with Al addition lead to a small λ and the increased energy consumption in dislocation migration. The decreased λ results in an increase in $\Delta\sigma_{\text{Orowan}}$, which is consistent with the significantly enhanced tensile strength in the tensile test. The refinement of grains also plays an important role in the optimization of mechanical property. The increased grain boundaries in the matrix also act as a strong hindrance for the movement of dislocations during the deformation. This phenomenon can be explained by the Hall-Petch model [35]. The refined grain size leads to an increase in the number of grain boundary in the matrix, and in turn hinders the movement of dislocations and improves the strength. In fact, the refinement of grain will induce lots of slip systems in ferrite-Fe matrix and improve the ductility during the plasticity deformation process. However, the hindrance of numerous second-phase particles plays a major role in plastic deformation mechanism, so that the ductility of ODS steel still remains a deteriorative trend.

Figure 8 shows SEM images of fracture surface of the ODS steels with different Al addition after the tensile test under room temperature. It can be seen that the tensile fracture of the ODS steel without Al addition contains a large sized dimple, which is clearly different from the fracture morphology of Al added ODS steels. The dimple facture mechanism in the steel without Al element is consistent with its excellent total elongation in tensile test. Due to the

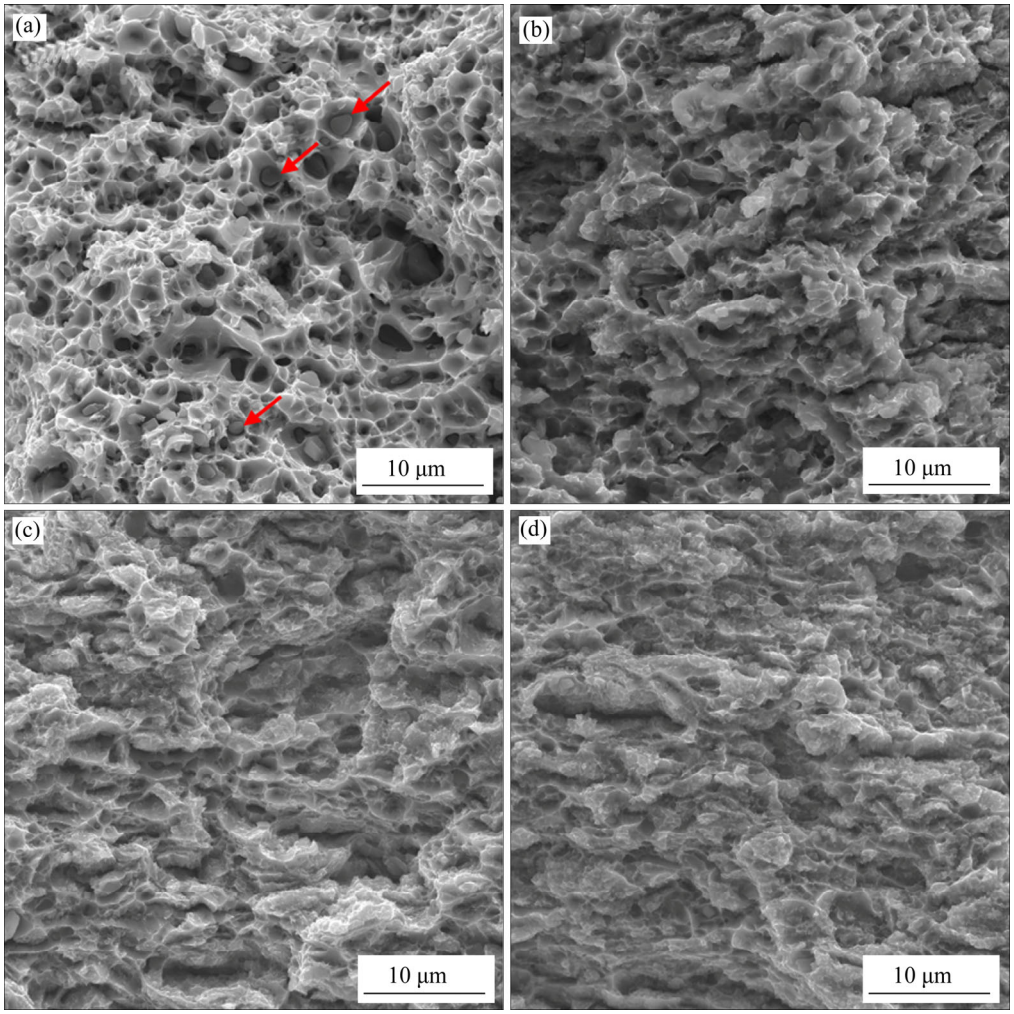

Figure 8 SEM images of fracture surfaces for specimens with 0 (a), 1 wt% (b), 2 wt% (c) and 3 wt% (d) Al additions

high sensitivity to stress of the interface, the crack propagation in the plastic deformation of matrix generally starts at the interface between the particles and the matrix. The red arrows as marked in Figure 8(a) denote the second-phase particles in the dimple area. As shown in Figures 8(b)−(d), the size and depth of dimples on fracture surface of the ODS steels with 1 wt%−3 wt% Al addition are significantly lower than those of the steel without Al addition. With increasing Al content, both the size and depth of dimples on fracture surface get small. Therefore, the appearance of fine oxide particles induced by Al addition is the main reason for hindering the plastic deformation during the tensile test and improving the tensile strength of ODS steels.

3.4 Corrosion resistance of Al-doped ODS steel

In order to investigate the corrosion resistance of Al-doped ODS steels, the potentiodynamic polarization curves of Al doped ODS steels in 1 mol/L HNO_3 solution at 55 °C are shown in Figure 9. The corrosion potential (E_{corr}) and passive current density (i_{pass}) obtained from the polarization curves are detailed in Table 2. Different polarization behaviors for ODS steels containing various Al element are investigated. The measured E_{corr} value of ODS steel without Al addition is −0.161 V. The increasing Al contents cause the raised corrosion potential of material. The E_{corr} values of material with 2 wt% and 3 wt% Al addition are 0.390 V and 0.492 V, respectively. Meanwhile, the i_{pass} values show a general downward trend with the elevated Al content. The increasing E_{corr} and decreasing i_{pass} signify the improved corrosion resistance. In polarization curves, the corrosion currents of samples show a stable feature when corrosion potential value maintains in 0.6−1.0 V and 1.2−1.6 V, which means the formation of Cr, Al oxide passive film on the surface of steel. The existence of passive film protects the matrix from continuous corrosion in nitric acid solution. It should be noted that the corrosion current of 15Cr1Al ODS steel exhibits a multiple reversing process and three corrosion potentials in the curve. Owing to the multi-potential in incomplete passivation or the formation of passive film in the unsteady status, two and three potentials can be found in polarization test of 9Cr ODS steels at nitric acid medium [36, 37].

The morphology of the corrosion surface of

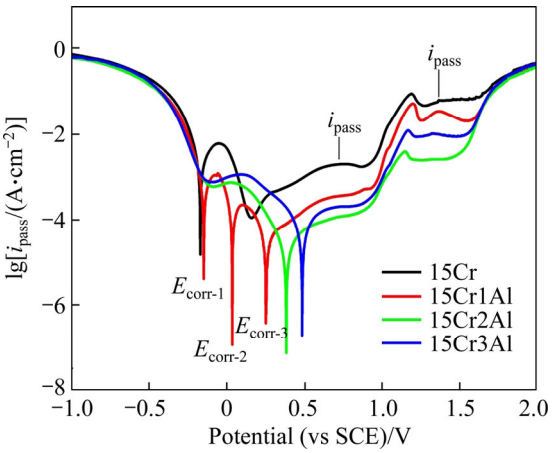

Figure 9 Potentiodynamic polarization curves of Al doped ODS steels in nitric acid solution at 55 °C

Table 2 Electrochemical parameters of ODS steels with different Al contents

Sample	E_{corr} (vs SCE)/V	i_{pass}/(A/cm^{-2})
15Cr	−0.161	2.02×10^{-3} (0.74 V) 6.323×10^{-2} (1.37 V)
15Cr1Al	−0.139 (E_{corr-1}) 0.044 (E_{corr-2}) 0.259 (E_{corr-3})	3.680×10^{-3} (0.74 V) 3.483×10^{-2} (1.37 V)
15Cr2Al	0.390	1.212×10^{-4} (0.74 V) 2.61×10^{-3} (1.37 V)
15Cr3Al	0.492	2.075×10^{-4} (0.74 V) 1.014×10^{-2} (1.37 V)

ODS steels with different Al contents after polarization test are shown in Figure 10. The corrosion situation of ODS steel revealed by SEM morphology is consistent with the corrosion current of materials in Table 2. In 0 and 1 wt% Al doped samples, a large amount of surfaces have been eroded and there are the coarse holes. Significantly, the deep corrosive hole appears in partial area of Al-free 15Cr ODS alloy. With the further elevated Al addition, the coarse pits disappear gradually and have been replaced by fine pits on the surface film. The improvement of corrosion resistance is attributed to the elevated content of Al element, which could form passive Al oxide film to protect the matrix from further attack by corrosive medium.

In order to determine the composition of corrosion surface, the XPS measurement of 15Cr2Al ODS steel after electrochemical tests was carried out. Figure 11(a) shows the wide scan survey spectrum of corroded surface of 15Cr2Al ODS steel. Fe, Cr, O, C, Al elements are identified in test procedure. Beside,

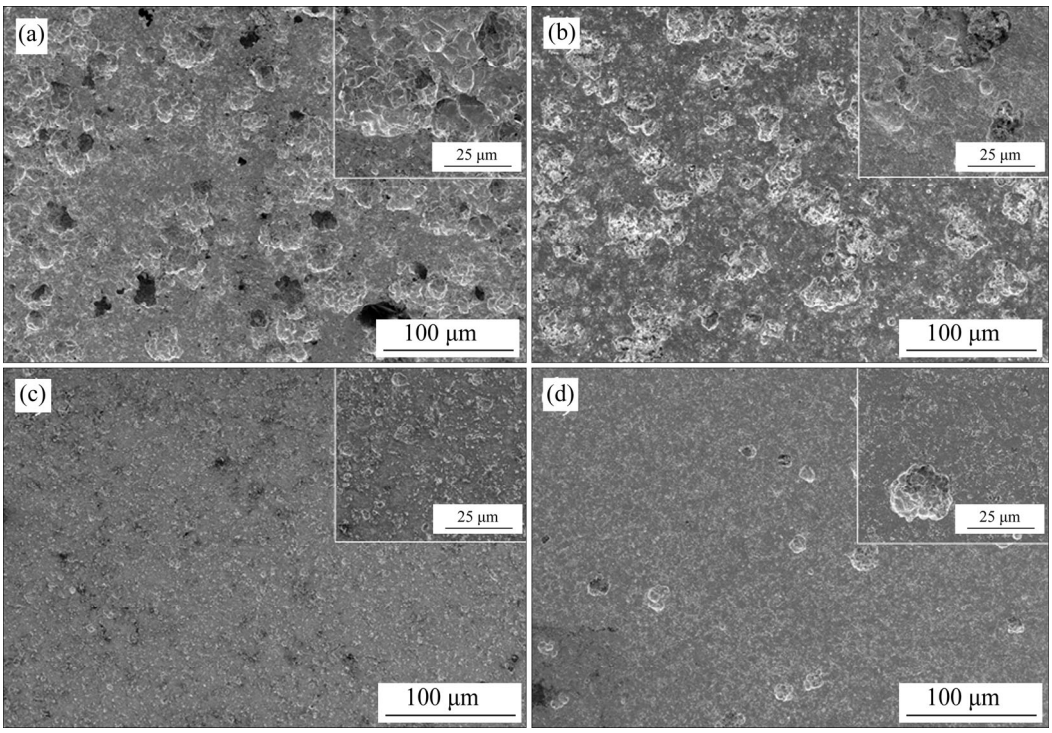

Figure 10 Typical SEM images of corrosion surface of ODS steels with different Al additions after potentiodynamic polarization test: (a) 0; (b) 1 wt%; (c) 2 wt%; (d) 3 wt%

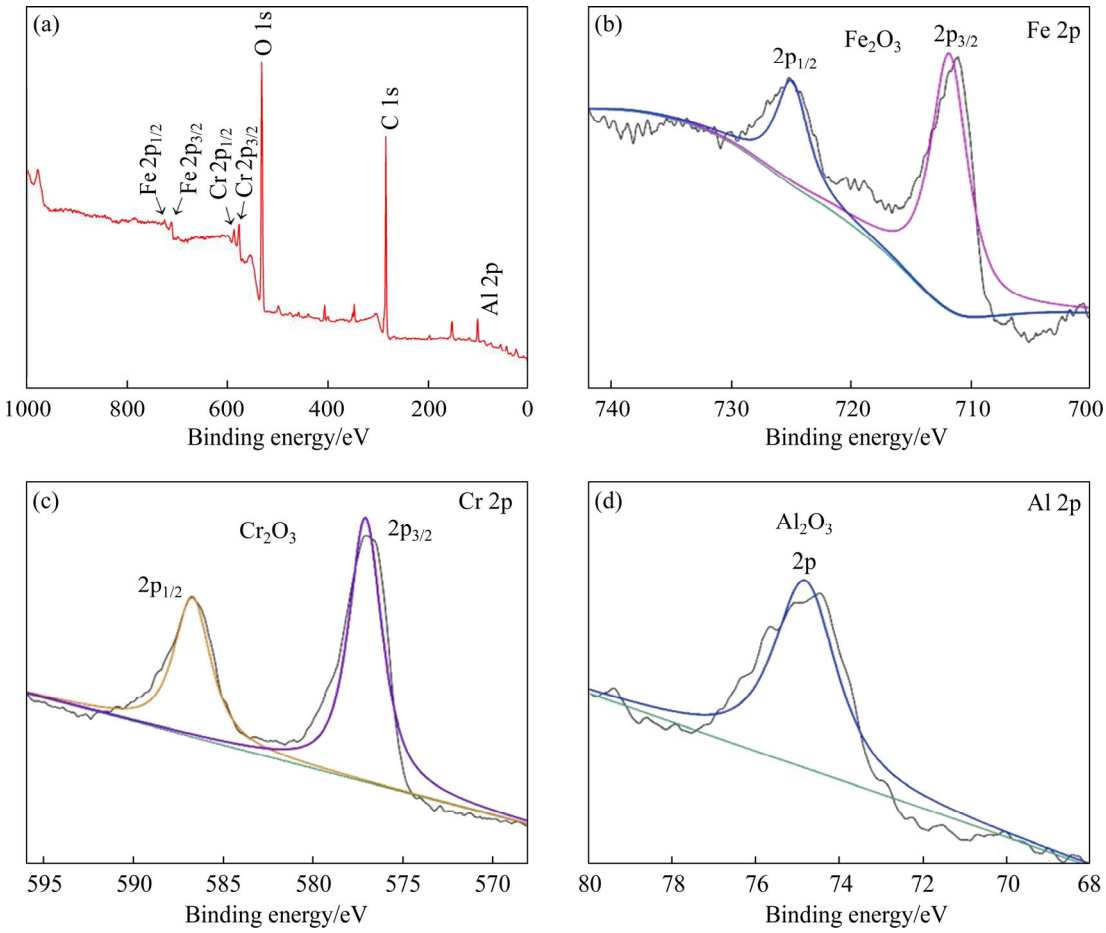

Figure 11 XPS spectrum (a) and corresponding products of Fe 2p (b), Cr 2p (c) and Al 2p (d) obtained from corroded surface of 15Cr2Al ODS steel in 1 mol/L HNO_3 nitric solution

XPS spectra of Fe 2p, Cr 2p and Al 2p are presented in Figures 11(b)−(d). The peaks of Fe 2p, Cr 2p and Al 2p in XPS spectrum indicate the formation of Fe_2O_3, Cr_2O_3 and Al_2O_3 during the corrosion process, respectively. Except for Cr_2O_3 in Al-doped ODS alloy, Al_2O_3 in passive film can hinder the metal dissolution during the anodic oxidation reaction, which causes the decreasing i_{pass} value and improved corrosion resistance. The composition of Al oxide enrichment was also determined to be Al_2O_3 in the previous literature, proving the high stability in an aggressive corrosive nitric acid environment [38, 39]. However, it is worth noting that the corrosion current of steel tends to increase slightly when Al content exceeds 2 wt%. The increasing second phase precipitates may induce an increment of corrosion current. The dispersion particles act as the initiation site of corrosion process, which induces the further dissolution of dispersion particles and matrix in nitric acid medium and results in the formation of pitting corrosion, as shown in Figure 10(d) [38, 40].

4 Conclusions

In summary, Al added ODS steels with excellent strength and toughness were successfully fabricated by combining the wet-milling and SPS sintering methods. The precipitate phase, microstructure and mechanical properties of Al added ODS steels were investigated systemically. It is found that the formation of Fe-Cr phase matrix and the dissolution of Al and W elements in the matrix occur at high temperature sintering stage. The addition of Al powders leads to a refinement of the oxide particles and the refining grain size of matrix. Both the small oxide particles and small Fe-Cr grains are responsible for the excellent mechanical property of the obtained ODS steels. The UTS and TE values of 15Cr3Al ODS alloy are much higher than those of the commercial MA956 ODS alloy. With the elevated Al content, the corrosion resistance of ODS steel in nitric acid solution is improved evidently. Therefore, our experimental findings demonstrate that the wet milling process may be a feasible way to prepare the ODS steels with excellent mechanical property.

Contributors

SUN Yu-zhou wrote the first draft of the manuscript. LIN Nan and MA Chao provided the concept and edited the draft of manuscript. SUN Yu-zhou, LI Zhong-tao, HAN Xian-qi, WU Zheng-gang and WANG Zu-yong prepared the materials and measured the properties of materials. MA Chao, ZHANG Wu-jun and ZHANG Yong-sen carried out TEM experiments. SUN Yu-zhou analyzed the measured data.

Conflict of interest

SUN Yu-zhou, LIN Nan, ZHANG Wu-jun, ZHANG Yong-sen, LI Zhong-tao, HAN Xian-qi, WU Zheng-gang, WANG Zu-yong and MA Chao declare that they have no conflict of interest.

References

[1] ODETTE G R, ALINGER M J, WIRTH B D. Recent developments in irradiation-resistant steels [J]. Annual Review of Materials Research, 2008, 38(1): 471−503. DOI: 10.1146/annurev.matsci.38.060407.130315.

[2] ZINKLE S J, SNEAD L L. Designing radiation resistance in materials for fusion energy [J]. Annual Review of Materials Research, 2014, 44(1): 241−267.

[3] KIMURA A, KASADA R, IWATA N, KISHIMOTO H, ZHANG C H, ISSELIN J, DOU P, LEE J H, MUTHUKUMAR N, OKUDA T, INOUE M, UKAI S, OHNUKI S, FUJISAWA T, ABE T F. Development of Al added high-Cr ODS steels for fuel cladding of next generation nuclear systems [J]. Journal of Nuclear Materials, 2011, 417(1−3): 176−179. DOI: 10.1016/j.jnucmat.2010.12.300.

[4] BISCHOFF J, MOTTA A T. Oxidation behavior of ferritic-martensitic and ODS steels in supercritical water [J]. Journal of Nuclear Materials, 2012, 424(1−3): 261−276.

[5] DUBUISSON P, DE CARLAN Y, GARAT V, BLAT M. ODS ferritic/martensitic alloys for sodium fast reactor fuel pin cladding [J]. Journal of Nuclear Materials, 2012, 428(1−3): 6−12. DOI: 10.1016/j.jnucmat.2011.10.037.

[6] ALLEN T R, CRAWFORD D C. Lead-cooled fast reactor systems and the fuels and materials challenges [J]. Science and Technology of Nuclear Installations, 2007: 097486. DOI: 10.1155/2007/97486.

[7] TAKAYA S, FURUKAWA T, AOTO K, MUELLER G, WEISENBURGER A, HEINZEL A, INOUE M, OKUDA T, ABE F, OHNUKI S, FUJISAWA T, KIMURA A. Corrosion behavior of Al-alloying high Cr-ODS steels in lead-bismuth eutectic [J]. Journal of Nuclear Materials, 2009, 386−388: 507−510. DOI: 10.1016/j.jnucmat.2008.12.155.

[8] ISSELIN J, KASADA R, KIMURA A. Corrosion behaviour of 16%Cr-4%Al and 16%Cr ODS ferritic steels under different metallurgical conditions in a supercritical water environment [J]. Corrosion Science, 2010, 52(10): 3266−3270. DOI: 10.1016/j.corsci.2010.05.043.

[9] KLIMIANKOU M, LINDAU R, MÖSLANG A, SCHRÖDER J. TEM study of PM 2000 steel [J]. Powder Metallurgy, 2013, 48(3): 277−287. DOI: 10.1179/174329005x64171.

[10] MEDRAJ M, HAMMOND R, PARVEZ M A, DREW R A L, THOMPSON W T. High temperature neutron diffraction study of the Al_2O_3-Y_2O_3 system [J]. Journal of the European Ceramic Society, 2006, 26(16): 3515−3524. DOI: 10.1016/j.jeurceramsoc.2005.12.008.

[11] DOU P, KIMURA A, OKUDA T, INOUE M, UKAI S, OHNUKI S, FUJISAWA T, ABE F. Polymorphic and coherency transition of Y-Al complex oxide particles with extrusion temperature in an Al-alloyed high-Cr oxide dispersion strengthened ferritic steel [J]. Acta Materialia, 2011, 59(3): 992−1002. DOI: 10.1016/j.actamat.2010.10.026.

[12] HSIUNG L L, FLUSS M J, TUMEY S J, CHOI B W, SERRUYS Y, WILLAIME F, KIMURA A. Formation mechanism and the role of nanoparticles in Fe-Cr ODS steels developed for radiation tolerance [J]. Physical Review B, 2010, 82(18): 184103. DOI: 10.1103/PhysRevB.82.184103.

[13] KASADA R, TODA N, YUTANI K, CHO H S, KISHIMOTO H, KIMURA A. Pre- and post-deformation microstructures of oxide dispersion strengthened ferritic steels [J]. Journal of Nuclear Materials, 2007, 367: 222−228. DOI: 10.1016/j.jnucmat.2007.03.141.

[14] ZHANG C H, KIMURA A, KASADA R, JANG J, KISHIMOTO H, YANG Y T. Characterization of the oxide particles in Al-added high-Cr ODS ferritic steels [J]. Journal of Nuclear Materials, 2011, 417(1−3): 221−224.

[15] CZYRSKA-FILEMONOWICZ A, DUBIEL B. Mechanically alloyed, ferritic oxide dispersion strengthened alloys: Structure and properties [J]. Journal of Materials Processing Technology, 1997, 64(1): 53−64.

[16] MILLER M K, HOELZER D T, KENIK E A, RUSSELL K F. Stability of ferritic MA/ODS alloys at high temperatures [J]. Intermetallics, 2005, 13(3, 4): 387−392. 10.1016/j.intermet.2004.07.036.

[17] DONG H, YU L, LIU Y, LIU C, LI H, WU J. Effect of hafnium addition on the microstructure and tensile properties of aluminum added high-Cr ODS steels [J]. Journal of Alloys and Compounds, 2017, 702: 538−545. DOI: 10.1016/j.jallcom.2017.01.298.

[18] XIE R, LU Z, LU C, LI Z, DING X, LIU C. Microstructures and mechanical properties of 9Cr oxide dispersion strengthened steel produced by spark plasma sintering [J]. Fusion Engineering and Design, 2017, 115: 67−73.

[19] ZHAO Q, QIAO Z, LIU Y, YU L, HUANG Y, GUO Q, LI H. Characterization of 14Cr ODS steel fabricated by spark plasma sintering [J]. Metals, 2019, 9(2): 200. DOI: 10.3390/met9020200.

[20] HUANG S G, LI L, VANMEENSEL K, van der BIEST O, VLEUGELS J. VC, Cr_3C_2 and NbC doped WC–Co cemented carbides prepared by pulsed electric current sintering [J]. International Journal of Refractory Metals and Hard Materials, 2007, 25(5, 6): 417−422.

[21] ZHANG Qian-kun, JIANG Yao, SHEN Wei-jun, ZHANG Hui-bin, HE Yue-hui, LIN Nan, LIU C T, HUANG Han, HUANG Xiao-lin. Direct fabrication of high-performance high speed steel products enhanced by LaB_6 [J]. Materials & Design, 2016, 112: 469−478.

[22] ZHAO L, LIN N, HE Y. Improvement in microstructure and properties of Ti(C,N)-based cermets with ruthenium additions [J]. Ceramics International, 2018, 44(14): 17553−17561. DOI: 10.1016/j.ceramint.2018.06.156.

[23] HE P, KLIMENKOV M, LINDAU R, MOSLANG A. Characterization of precipitates in nano structured 14% Cr ODS alloys for fusion application [J]. Journal of Nuclear Materials, 2012, 428(1−3): 131−138.

[24] ZHANG G, ZHOU Z, MO K, WANG P, MIAO Y, LI S, WANG M, LIU X, GONG M, ALMER J, STUBBINS J F. The microstructure and mechanical properties of Al-containing 9Cr ODS ferritic alloy [J]. Journal of Alloys and Compounds, 2015, 648: 223−228. DOI: 10.1016/j.jallcom.2015.06.214.

[25] KUMAR P K, SAI N V, KRISHNA A G, RENGANATHAN N G. Fabrication and micro-structural evaluation of ODS austenitic stainless steels through mechanical alloying [J]. Materials Today: Proceedings, 2020, 23: 465−468. DOI: 10.1016/j.matpr.2019.04.207.

[26] MIHALACHE V, MERCIONIU I, VELEA A, PALADE P. Effect of the process control agent in the ball-milled powders and SPS-consolidation temperature on the grain refinement, density and Vickers hardness of Fe14Cr ODS ferritic alloys [J]. Powder Technology, 2019, 347: 103−113. DOI: 10.1016/j.powtec.2019.02.006.

[27] BHATTACHARYYA D, DICKERSON P, ODETTE G R, MALOY S A, MISRA A, NASTASI M A. On the structure and chemistry of complex oxide nanofeatures in nanostructured ferritic alloy U14YWT [J]. Philosophical Magazine, 2012, 92(16): 2089−2107.

[28] RAO K R, SINHA S K. Effect of sintering temperature on microstructural and mechanical properties of SPS processed CoCrCuFeNi based ODS high entropy alloy [J]. Materials Chemistry and Physics, 2020, 256: Article 123709.

[29] LU C, LU Z, XIE R, LIU C, WANG L. Microstructure of a 14Cr-ODS ferritic steel before and after helium ion implantation [J]. Journal of Nuclear Materials, 2014, 455(1−3): 366−370. DOI: 10.1016/j.jnucmat.2014.06.065.

[30] KLIMENKOV M, MÖSLANG A, LINDAU R. EELS analysis of complex precipitates in PM 2000 steel [J]. The European Physical Journal Applied Physics, 2008, 42(3): 293−303.

[31] LIU T, WANG L, WANG C, SHEN H, ZHANG H. Feasibility of using $Y_2Ti_2O_7$ nanoparticles to fabricate high strength oxide dispersion strengthened Fe–Cr–Al steels [J]. Materials & Design, 2015, 88: 862−870.

[32] CASAS C, TEJEDOR R, RODRÍGUEZ- BARACALDO R, BENITO J A, CABRERA J M. The effect of oxide particles on the strength and ductility of bulk iron with a bimodal grain size distribution [J]. Materials Science and Engineering A, 2015, 627: 205−216.

[33] KLUEH R L, SHINGLEDECKER J P, SWINDEMAN R W, HOELZER D T. Oxide dispersion-strengthened steels: A comparison of some commercial and experimental alloys [J]. Journal of Nuclear Materials, 2005, 341(2, 3): 103−114. DOI: 10.1016/j.jnucmat.2005.01.017.

[34] ZHANG Z, CHEN D. Consideration of Orowan strengthening effect in particulate-reinforced metal matrix nanocomposites: A model for predicting their yield strength [J]. Scripta Materialia, 2006, 54(7): 1321−1326.

[35] HALL E O. The deformation and ageing of mild steel: III Discussion of results [J]. Proceedings of the Physical Society. Section B, 1951, 64(9): 747−753. DOI: 10.1088/0370-

1301/64/9/303.

[36] NINGSHEN S, SAKAIRI M, SUZUKI K, UKAI S. The surface characterization and corrosion resistance of 11% Cr ferritic/martensitic and 9–15 % Cr ODS steels for nuclear fuel reprocessing application [J]. Journal of Solid State Electrochemistry, 2013, 18(2): 411−425. DOI: 10.1007/s10008-013-2165-5.

[37] NINGSHEN S, SAKAIRI M, SUZUKI K, UKAI S. Corrosion resistance of 9% Cr oxide dispersion-strengthened steel in different electrolytic media [J]. Corrosion, 2013, 69(9): 863−874.

[38] PRIYA R, NINGSHEN S, SAKAIRI M, UKAI S. Corrosion behaviour of Al-containing high Cr ferritic oxide dispersion strengthened steel in nitric acid environment [J]. Journal of Nuclear Materials, 2020, 534. DOI: 10.1016/j.jnucmat.2020.152120.

[39] ZHAO H, LIU T, BAI Z, WANG L, GAO W, ZHANG L. Corrosion behavior of 14Cr ODS steel in supercritical water: The influence of substituting Y_2O_3 with Y2Ti2O7 nanoparticles [J]. Corrosion Science, 2020, 163. DOI: 10.1016/j.corsci.2019. 108272.

[40] NAGINI M, JYOTHIRMAYI A, VIJAY R, RAO T N, REDDY A V, RAJULAPATI K V, SUNDARARAJAN G. Influence of dispersoids on corrosion behavior of oxide dispersion-strengthened 18cr steels made by high-energy milling [J]. Journal of Materials Engineering Performance, 2016, 25(2): 577−586. DOI: 10.1007/s11665-015-1859-5.

(Edited by HE Yun-bin)

中文导读

湿磨与 SPS 烧结制备 Al 添加 ODS 钢的显微组织结构与力学性能研究

摘要：本文利用湿磨和放电等离子烧结技术制备了 Al 含量分别为 0，1 wt%，2 wt%和 3 wt%的 15Cr-ODS 钢。通过 XRD、SEM、TEM、EBSD 和拉伸测试等对 ODS 钢的显微组织结构与力学性能进行了研究。研究结果表明，Al 元素的添加能够显著细化 Fe-Cr 相基体中的析出相颗粒，减小基体晶粒尺寸并改善材料的力学性能。Al 添加 ODS 钢基体中尺寸为 5~300 nm 的弥散颗粒可以被标定为 Al_2O_3 与 $Y_2Ti_2O_7$ 纳米粒子，这些弥散颗粒的尺寸分布较为不均匀。随着 Al 元素添加量的增加，材料的伸长率降低，但其抗拉强度显著的提升。当 Al 元素添加量为 3 wt%时，15Cr3Al-ODS 钢抗拉强度与伸长率分别为 775.3 MPa 和 15.1%。Al 元素的添加还可增强材料的耐腐蚀性能，Al 含量为 2 wt%ODS 钢的腐蚀电位(E_{corr})与钝化电流密度(i_{pass})分别为 0.39 V 和 2.61×10^{-3} A/cm^2 (1.37 V)。因此，本文使用湿磨和放电等离子烧结方法制备的 Al 添加 ODS 钢在核能系统结构部件中能够具有良好的应用前景。

关键词：ODS 钢；氧化物纳米粒子；微观结构；拉伸强度；弥散强化